Quenched magneto-association of ultracold Feshbach molecules

Kirk Waiblinger[1], Jason R. Williams,[2] and José P. D'Incao[1,3]

[1]*Department of Physics, University of Colorado, Boulder, 80309 Colorado, USA*
[2]*Jet Propulsion Laboratory, California Institute of Technology, Pasadena, 91011 California, USA*
[3]*JILA, University of Colorado and NIST, Boulder, 80309 Colorado, USA*

We study enhanced magneto-association of atoms into weakly bound molecules near a Feshbach resonance using a quench preparatory stage. In anticipation of experiments with NASA's Cold Atom Laboratory aboard the International Space Station, we assume as a baseline a dual-species (^{87}Rb and ^{41}K) gas in a parameter regime enabled by a microgravity environment. It includes subnanokelvin temperatures and dual-species gases at densities as low as $10^8/\text{cm}^3$. Our studies indicate that, in such a regime, traditional magneto-association schemes are inefficient due to the weak coupling between atomic and molecular states at low densities, thus requiring extremely long magnetic field sweeps. To address this issue we propose a modified scheme in which atoms are quenched to unitarity before proceeding with magneto-association. This modified scheme substantially improves molecular formation, allowing for up to 80% efficiency within timescales much shorter than those associated with atomic and molecular losses. We show that this scheme also applies at higher densities, therefore proving to be of interest in ground-based experiments as well.

I. INTRODUCTION

Ultracold molecules are today one of the physical systems most used to study a variety of physical phenomena, ranging from quantum information [1–5] to ultracold chemistry [6–9], exploration of novel dipolar phases of matter [10–15], and tests of variations of fundamental constants [16–18]. As a result, developing efficient techniques to produce such molecules is a highly sought after goal [19–25]. Since most experiments using such molecules start from a gas of ultracold atoms, the central question is how to efficiently produce a dense sample of molecules while still keeping them at ultracold temperatures. Magneto-association provides such a path and has been routinely implemented in a broad range of molecular experiments to date [26–31]. In this scheme, atoms are exposed to a magnetic field B tuned near a Feshbach resonance, causing the s-wave scattering length a to go through a pole and causing interactions to become extremely strong [32]. Sweeping the magnitude of the B field across the resonance will convert atoms adiabatically to weakly bound Feshbach molecules, which exist for $a > 0$. Feshbach molecules can then be further used to explore a variety of phenomena or can be used as an intermediate state to form more deeply bound molecular species by using other association schemes like stimulated Raman adiabatic passage [33].

The efficiency of magneto-association is fundamentally controlled by the B-field sweeping rates but also depends on the initial atomic densities and temperatures [26–31], as well as depending nontrivially on the microscopic details characterizing the interatomic interactions [19,20]. For NASA's Cold Atom Laboratory (CAL), a multiuser facility aboard the International Space Station [34,35], the microgravity environment will provide experimental conditions vastly different from those achievable in ground-based experiments exploring magneto-association. Here, we will show that although the unique experimental conditions available at CAL favor high phase-space density, long interrogation times, and suppression of gravitation sag, the ultralow atomic densities ($n = 10^8–10^{11}/\text{cm}^3$) desired for various proposed experiments will drastically affect the efficiency of magneto-association. At such low densities, as opposed to those typically found in ground-based experiments ($n = 10^{12}/\text{cm}^3$ and higher), the required B-field sweeps to obtain satisfactory efficiency are simply too slow, compromising the stability of the molecular sample against three-body losses. A similar scenario is also found near narrow Feshbach resonances where atomic and molecular states are naturally weak. This issue is of particular importance for studies of dual-species atom interferometry in which the formation of heteronuclear Feshbach molecules [24] is of fundamental interest to mitigate some of the major sources of systematic errors for high-precision tests of fundamental physics [36–38].

In order to optimize the formation of Feshbach molecules, we modify the traditional magneto-association (TMA) scheme. Our scheme adds a preparatory stage where the B field is changed abruptly (quenched) from off resonance to on resonance and then is allowed to dwell in this regime while developing correlations. This strongly correlated state will now serve as the initial state for magneto-association, providing a much higher overlap with the desired final molecular states. This scheme is similar to the one used for ^{85}Rb in Ref. [39] which provided association of not only dimers but also Efimov trimers [40]. We show that this scheme, which we defined as quenched magneto-association (QMA), substantially

improves the efficiency of molecule formation in the ultralow density regime while still allowing it to be performed within timescales much shorter than those associated with atomic and molecular losses. Our proposed QMA is also found to be superior to TMA at higher densities, thus being of interest for ground-based experiments. More generally, we conjecture that QMA can also be potentially useful for molecular association studies near narrow Feshbach resonances since it provides a scheme to produce a strongly correlated state for association regardless of the strength of the resonance. Keeping in mind the relevant case of ^{87}Rb-^{41}K mixtures available at CAL, our paper is organized as follows. In Sec. II we describe our theoretical model and emphasize its main assumptions and approximations. Section III details both TMA and QMA schemes and analyzes the important timescales associated with the atomic and molecular losses. In Sec. IV we present our results for the association of ^{87}Rb^{41}K Feshbach molecules and discuss the main advantages of QMA while verifying its fundamental differences from TMA schemes.

II. THEORETICAL MODEL

In this study we adopted two major assumptions that allow for a qualitative description of magneto-association while still providing a clear physical picture of how the medium (density) affects the association process. For the interatomic interactions we assume a single-channel interaction model between ^{87}Rb and ^{41}K atoms, given by a Lennard-Jones potential,

$$v(r) = -\frac{C_6}{r^6}\left(1 - \frac{\lambda^6}{r^6}\right),$$ (1)

where $C_6 \approx 4274a_0^6 E_h$ [41] is the van der Waals dispersion coefficient and λ is a tunable parameter adjusted to provide the desired value of the scattering length. A more realistic description of the interactions between alkali atoms, however, is multichannel in nature and includes the hyperfine interactions responsible for the B-field dependence of the scattering length used in experiments with Feshbach resonances. A single-channel description of this phenomenon is supported by the universal properties of the system [32] whenever $|a| \gg r_{\mathrm{vdW}}$, where $r_{\mathrm{vdW}} = (2\mu C_6/\hbar^2)^{1/4}/2$ is the van de Waals length and μ is the two-body reduced mass. In our present study we model the ^{87}Rb-^{41}K interactions near the well-known Feshbach resonance for atoms in the $|f = 1, m_f = 1\rangle$ hyperfine state (see Fig. 1) by adjusting the values of λ in Eq. (1) for each value of B to produce the same value of a. As usual, for B fields near a Feshbach resonance the scattering length is well represented by

$$a(B) = a_{\mathrm{bg}}\left(1 - \frac{\Delta B}{B - B_0}\right),$$ (2)

where the position of the resonance is $B_0 \approx 39.4$ G, its width $\Delta B \approx 37$ G, and background scattering length $a_{\mathrm{bg}} \approx 284a_0$ [42].

In order to incorporate density effects to properly describe magneto-association in ultracold quantum gases, we have employed the local-density model [43–48], allowing for a physically meaningful way to qualitatively describe the density dependence of various few-body observables. This model
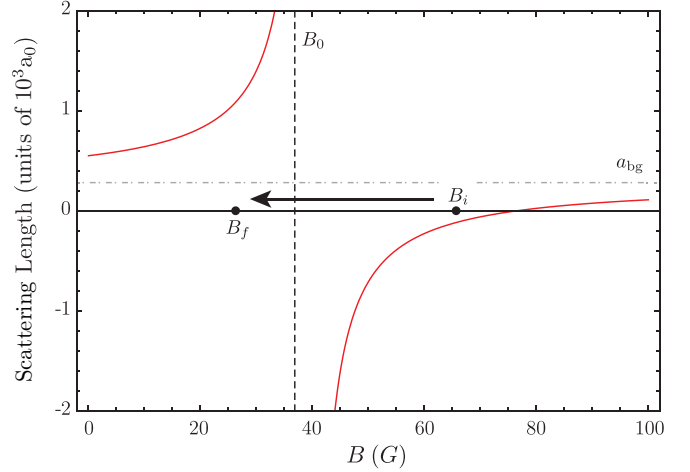

FIG. 1. Scattering length (in units of the Bohr radius a_0) as a function of applied B field near the ^{87}Rb-^{41}K Feshbach resonance at $B_0 \approx 39.4$ G. This resonance is characterized by a width $\Delta B \approx 37$ G and background scattering length $a_{\mathrm{bg}} \approx 284a_0$ [42]. Both ^{87}Rb and ^{41}K atoms are in the $|f = 1, m_f = 1\rangle$ hyperfine state. B_i and B_f indicate, respectively, the initial and final values of the B field in a hypothetical magneto-association scheme.

introduces a harmonic confinement to the few-body Hamiltonian, whose strength is adjusted to produce a few-body "density" that matches that of the experiment. In our current study, the two-atom Hamiltonian is then written as

$$\hat{H} = -\frac{\hbar^2}{2\mu}\nabla^2 + \frac{\hbar^2}{8\mu a_{ho}^4}r^2 + v(r),$$ (3)

where a_{ho} is the harmonic oscillator length. We assume that the number densities of Rb and K are equal, i.e., $n_{\mathrm{Rb}} = n_{\mathrm{K}} = n$, and relate the oscillator length to the number density as [46]

$$a_{ho} = \sqrt{\frac{\pi}{8}}\left(\frac{4\pi n}{3}\right)^{-1/3}.$$ (4)

This relation allows us to connect our few-body analysis with the relevant energy, length, and timescales to the macroscopic system characterized by, respectively,

$$E_n = \frac{(6\pi^2 n)^{2/3}}{2\mu}\hbar^2, \quad k_n = \frac{\sqrt{2\mu E_n}}{\hbar}, \quad t_n = \frac{\hbar}{E_n}.$$ (5)

We note that our model does not take into account quantum degeneracy and phase-space density effects for association of Feshbach molecules such as those experimentally observed in Refs. [49–51]. Nevertheless, the qualitative aspects of our analysis (in particular, the comparison between TMA and QMA protocols) still persist and should be observed in more elaborate models in which such collective effects are properly accounted for.

As a result, within our model magneto-association can easily be visualized through the two-atom energy spectrum, as shown in Fig. 2. The horizontal energy levels in the $1/|k_n a| \gg 1$ regime correspond to harmonic states and represent noninteracting atom states. The desired target Feshbach molecular state is that with energy given by $-E_b = -\hbar^2/2\mu a^2$ for $a > 0$ and is also indicated in Fig. 2. [The energy spectrum is
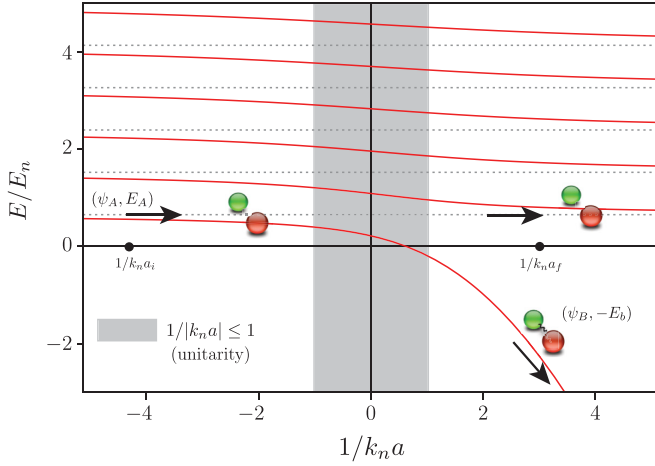
FIG. 2. The energy levels of two atoms in a harmonic trap parameterized by $1/k_n a$ and orbital angular momentum $l = 0$ (see text). In the limit of large $1/|k_n a|$, the spectrum consists of pure harmonic oscillator levels, whose energies are plotted as dashed lines. Positive energies correspond to atomic states, and negative energies represent molecular states. Note that the expected Feshbach molecular state for large positive a, having binding energy $E_b = \hbar^2/2\mu a^2$, is shifted slightly due to the oscillator potential. The gray region indicate the values in which the system is found in the unitary regime, $1/|k_n a| < 1$.

obtained by solving the two-body Schrödinger equation for the Hamiltonian in Eq. (3) for the lowest angular momentum state, $l = 0$.] The effect of sweeping the B field from high to low (from B_i to B_f in Fig. 1) corresponds to sweeping $1/k_n a$ from left to right (from $1/k a_i$ to $1/k_n a_f$) in Fig. 2. Transitions from atomic to molecular states are stronger in the *interaction region* $1/|k_n a| \lesssim 1$, i.e., when interactions are unitary, $n|a|^3 \gtrsim 1$. Therefore, within our physical picture, magneto-association reduces to the problem of nonadiabatic crossing of energy levels (Landau-Zener) [52]. In our case, multiple levels can participate in the process. Nevertheless, the Landau-Zener (two-level) model still provides a qualitative interpretation of the phenomena and can serve as a guide for understanding of the important parameters controlling molecular association. For instance, within the Landau-Zener model [52] the probability of transitioning from energy level ϵ_1 to ϵ_2 via a linear sweep, $\epsilon_1 - \epsilon_2 = \alpha_\epsilon t$, where α_ϵ is the sweeping rate, is given by

$$P_{LZ} = 1 - e^{-2\pi\Gamma}. \tag{6}$$

Here, $\Gamma = \epsilon_{12}^2/\hbar\alpha_\epsilon$, with ϵ_{12} being the coupling between states ϵ_1 and ϵ_2. Applying this picture to our case in Fig. 2, where energies are given in units of E_n (5), allows us to access important information. For instance, since efficient association is obtained for $\Gamma \gg 1$, the sweeping rates are required to be $\alpha_\epsilon \propto n^{4/3}$, which can be too slow in the ultralow density regime of CAL. We will explore these issues next and provide an alternative approach to circumvent this limitation.

III. QUENCHED MAGNETO-ASSOCIATION

As already anticipated from the discussion in the previous section, TMA schemes, i.e., applying a linear B-field sweep

across a Feshbach resonance, might be inefficient for the low-density regime relevant for a microgravity environment. Here, we detail TMA, and we discuss an alternative scheme that overcomes its limitations but can also be applied to ground-based experiments. We also discuss and characterize atomic and molecular losses.

A. Sweeps and quenches

Within our model, the key physical aspect that makes TMA inefficient at low densities is the fact that during the B-field sweep the system remains in the interaction region, $1/|k_n a| \lesssim 1$, for a too short amount of time, thus requiring slow sweeps. The TMA scheme is illustrated in Fig. 3(a), where the B-field is linearly swept from B_i to B_f during a time t_{sw}. In order to determine the interaction time t_u, we assume $B(t) = B_i - \alpha_B t$, where $\alpha_B = |B_f - B_i|/t_{sw} \approx 26.03$ G/t_{sw} is the sweep rate, and determine values of B from Eq. (2) in which the condition $1/|k_n a| \lesssim 1$ is satisfied. After some algebra we arrive at the interaction time given by

$$t_u \approx 2\left|\frac{(k_n a_{bg})\Delta}{\alpha_B}\right| \propto n^{1/3} t_{sw}. \tag{7}$$

As a result, during a given sweep, atoms in the relevant states interact only during a much reduced amount of time as $n \to 0$.

In order to improve the interaction time and, consequently, the association efficiency, we propose the scheme illustrated in Fig. 3(b). In such a scheme, the system is first quenched to $1/|k_n a| = 0$, corresponding to changing the B field from B_i to B_0 within timescales much shorter than t_n. We note that at low densities the technical aspects of quenching the B field become increasingly easier since t_n increases as n decreases. For our studies we assume that the quench is performed instantaneously. After the quench, we allow the system to dwell for a time t_{dw} at $1/|k_n a| = 0$, thus letting interactions evolve before finally sweeping the field to its final value, B_f, according to $B(t) = B_0 - \alpha_B^* t$, where $\alpha_B^* = |B_f - B_0|/t_{sw} \approx 1.51$ G/t_{sw}. As a result, in QMA the interaction time is now given by

$$t_u^* = t_{dw} + \frac{t_u}{2} = t_{dw} + \underbrace{\left|\frac{(k_n a_{bg})\Delta}{\alpha_B^*}\right|}_{\propto n^{1/3} t_{sw}}, \tag{8}$$

which can be substantially enhanced by controlling t_{dw}. We note that this scheme is also similar to the one explored in Ref. [31], although assuming $t_{dw} \approx 0$ and obtaining an efficiency of about 30% at densities of 10^{12}/cm³.

Numerically, we study both TMA and QMA using the time-propagation methodology developed in Refs. [40,53], with a few caveats introduced by the quench. For TMA the initial state for propagation is a pure state; that is, it is given by

$$\Psi_i \equiv \psi_A^{a=a_i}(\mathbf{r}), \tag{9}$$

where ψ_A is an eigenstate of energy E_A for $a = a_i$ (see Fig. 2). In the quenched case, however, the initial state for propagation is instead a superposition of states given by

$$\Psi_i \equiv \sum_\beta c_\beta \exp\left[-\frac{iE_\beta t_{dw}}{\hbar}\right] \psi_\beta^{a=\pm\infty}(\mathbf{r}), \tag{10}$$
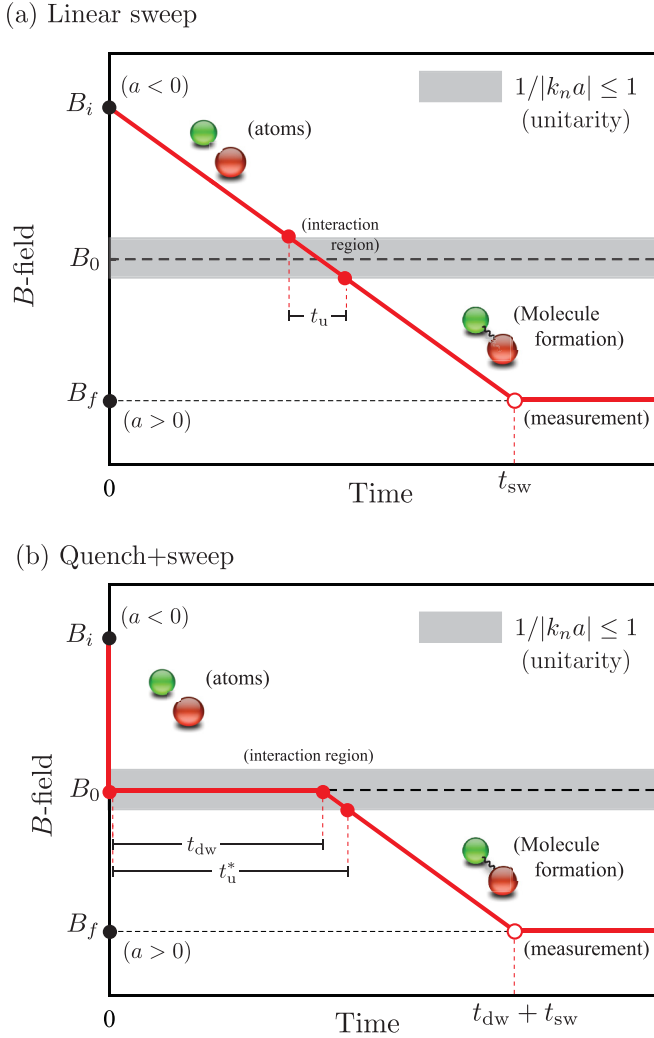
(a) Linear sweep

(b) Quench+sweep

FIG. 3. Schematic of magnetic field vs time in the traditional and quenched magneto-association schemes. (a) In the traditional magneto-association (TMA) B field is swept from B_i to B_f at a constant rate during a time t_{sw}. (b) In the quenched magneto-association (QMA) the B field is instantaneously quenched from B_i to B_0, remaining at $1/|k_n a| = 0$ for a dwell time t_{dw}, followed by a linear sweep from B_0 to B_f. This schematic figure is not to scale, and B_i and B_f will not, in general, be equidistant from B_0, nor will t_{sw} and t_{dw} bear any particular relationship to each other. Here, t_u and t_u^* represent the interaction time, i.e., the time in which $1/|k_n a| < 1$, for TMA and QMA, respectively.

where $c_\beta = \langle \psi_A | \psi_\beta \rangle$, with ψ_β and E_β being the eigenstates and energies of the system at $a = \pm\infty$. As we will see in Sec. IV, the dependence on t_{dw} in this state plays a crucial role that improves the efficiency of magneto-association by letting interactions evolve at $1/k_n a = 0$. Note also that for $t_{dw} \gg t_n$ we expect that truly many-body effects take place, potentially playing a role in QMA. Current models do not capture this physics properly, so we will keep our study within modest values of t_{dw}. Before we compare in detail both the TMA and QMA schemes in Fig. 3, we must first analyze the stability of the system with respect to losses, as done in the next section.

B. Atomic and molecular losses

Regardless of the particular magneto-association scheme adopted, few-body losses can drastically reduce the efficiency of molecule formation. Although such loss processes are, in general, well understood in ultracold atomic and molecular gases [54], magneto-association is a dynamical process, and the full understanding of how losses occur as the interactions evolve is nontrivial. In this section, however, we present an analysis that offers a qualitative understanding of the major loss processes, thus helping us to characterize and identify experimental regimes that are likely to mitigate their harmful effects.

In magneto-association the two major few-body loss processes are three-body recombination, the process in which three free atoms collide to produce an atom and a diatomic molecule, and atom-molecule vibrational relaxation, causing a deexcitation of the molecular state. Both processes release enough kinetic energy to make their products escape from typical traps [54]. In order to gain some insight into the timescales of the loss rates and their dependence on the experimentally relevant parameters, we consider the loss rates only in the regime at which they are maximal, i.e., $1/|k_n a| < 1$, which is the regime most relevant to magneto-association. This analysis should provide an upper limit for the lifetime of the sample during the magneto-association process.

It is well known that the three-body recombination rate in the regime $1/|k_n a| < 1$ becomes independent of the scattering length and is estimated as [54]

$$L_3^u(T) = \frac{4\pi^2 \hbar^5}{\mu_{3b}^3 (k_B T)^2}(1 - e^{-4\eta}), \qquad (11)$$

where $\mu_{3b}^2 = m_1 m_2 m_3 / (m_1 + m_2 + m_3)$ is the three-body reduced mass, T is the temperature, and η is the three-body inelasticity parameter, which provides a measure of the probability for inelastic transitions. The parameter η is dependent upon the details of the interactions and is, in general, obtained experimentally. For the Rb-K mixture we are interested here, Ref. [55] determined $\eta \approx 0.12$ for collisions involving two Rb atoms and one K (RbRbK) and $\eta \approx 0.02$ for collisions involving two K atoms and one Rb (KKRb). Now, assuming that the B-field sweep in TMA is performed at constant temperature, the atomic lifetime is given by

$$\tau_u(A) = \frac{1}{n^2 L_3^u(T)}$$
$$= \frac{9\pi^2 (k_B T)^2 \mu_{3b}^3}{8(1 - e^{-4\eta})\mu^3 \hbar^2} t_n^3 \propto \frac{(k_B T)^2}{n^2}, \qquad (12)$$

thus becoming shorter as the density increases and/or the temperature decreases. As a practical example, the lifetimes due to RbRbK losses at $T = 100$ pK and densities of $10^8/\text{cm}^3$, $10^9/\text{cm}^3$, $10^{10}/\text{cm}^3$, and $10^{11}/\text{cm}^3$ are, respectively, $37t_n$, $1.7t_n$, $0.08t_n$, and $0.0037t_n$, or, equivalently, 1 s, 10 ms, 0.1 ms, and 1 μs. In order to qualitatively understand what these lifetimes mean, the timescale of losses needs to be compared to that of the interaction time [Eq. (7)],

$$\tau_u(A)/t_u \propto \frac{(k_B T)^2}{n^{7/3} t_{sw}}. \qquad (13)$$

This indicates that an increase in the density or a decrease in temperature must be accompanied by a decrease of the sweeping time t_{sw} or, equivalently, an increase of the sweep rate α_B in order to compensate for the increase of atomic losses. As a result, since faster B-field sweeps reduce efficiency, obtaining a good balance of losses and interaction time, $\tau_u/t_u > 1$, can be done only at the risk of compromising efficiency. This makes it evident that finding the best regime for TMA is dependent upon a balance of various factors. Figure 4 shows the values for τ_u/t_u calculated from the lifetimes due to RbRbK losses at $T = 100$ pK (black dashed curves) for various densities and a broad range of sweeping times. Note that as n increases, the values of t_{sw} in which $\tau_u/t_u > 1$ quickly become more restrictive. For each density, we have indicated the corresponding values of E_n and t_n in relevant units.

In the case of QMA the key difference that improves the timescales for losses is that the quench itself increases the gas temperature and, according to Eq. (11), reduces the loss rates. Assuming that the initial temperature is smaller than E_n, the quench sets the temperature to $k_B T = E_n$ [56], thus leading to an atomic lifetime determined by

$$
\tau_u^*(A) = \frac{1}{n^2 L_3^u(E_n/k_B)}
$$
$$
= \frac{9\pi^2 \mu_{3b}^3}{8(1 - e^{-4\eta})\mu^3} t_n \propto \frac{1}{n^{2/3}}. \tag{14}
$$

Interestingly, the lifetime now is linearly proportional to t_n and, consequently, automatically rescales for different densities and provides a weaker dependence on density than Eq. (12). For instance, now the lifetime due to RbRbK losses at $T = 100$ pK is $295 t_n$, which for densities of $10^8/cm^3$, $10^9/cm^3$, $10^{10}/cm^3$, and $10^{11}/cm^3$ becomes 8 s, 1.7 s, 370 ms, and 80 ms, respectively. Comparing this lifetime to the interaction time in Eq. (8), we obtain in the limit of long dwell times, $t_{dw} \gg t_u$, an interaction time of $t_u^* \approx t_{dw}(\propto t_n)$, and

$$
\tau_u^*(A)/t_u^* \propto \text{const}. \tag{15}
$$

On the other hand, in the limit of short dwell times, $t_{dw} \ll t_u$, the interaction time is $t_u^* \approx t_u/2(\propto t_n)$, and

$$
\tau_u^*(A)/t_u^* \propto \frac{1}{n^{2/3} t_{sw}}. \tag{16}
$$

In either case, the above analysis indicates that QMA provides a substantially more favorable regime with respect to the scaling of losses with density and sweeping times. Figure 4 illustrates this more favorable conditions for QMA by displaying the values for τ_u^*/t_u^*, also calculated from the lifetimes due to RbRbK (solid curves), for various values of t_{dw}. Note that regardless of the density, a broad range of t_{sw} satisfies the favorable condition for association, $\tau_u^*/t_u^* > 1$, a result much superior to those from TMA.

A similar analysis of the lifetime can also be provided once molecular association takes place and the relevant loss process is atom-molecule relaxation. Here, too, loss rates in the regime $1/|k_n a| < 1$ become independent of the scattering length and are estimated as [54]

$$
\beta_u(T) = \frac{2^{1/2} \pi^{1/2} \hbar}{\mu_{ad}^{3/2}(k_B T)^{1/2}}(1 - e^{-4\eta}), \tag{17}
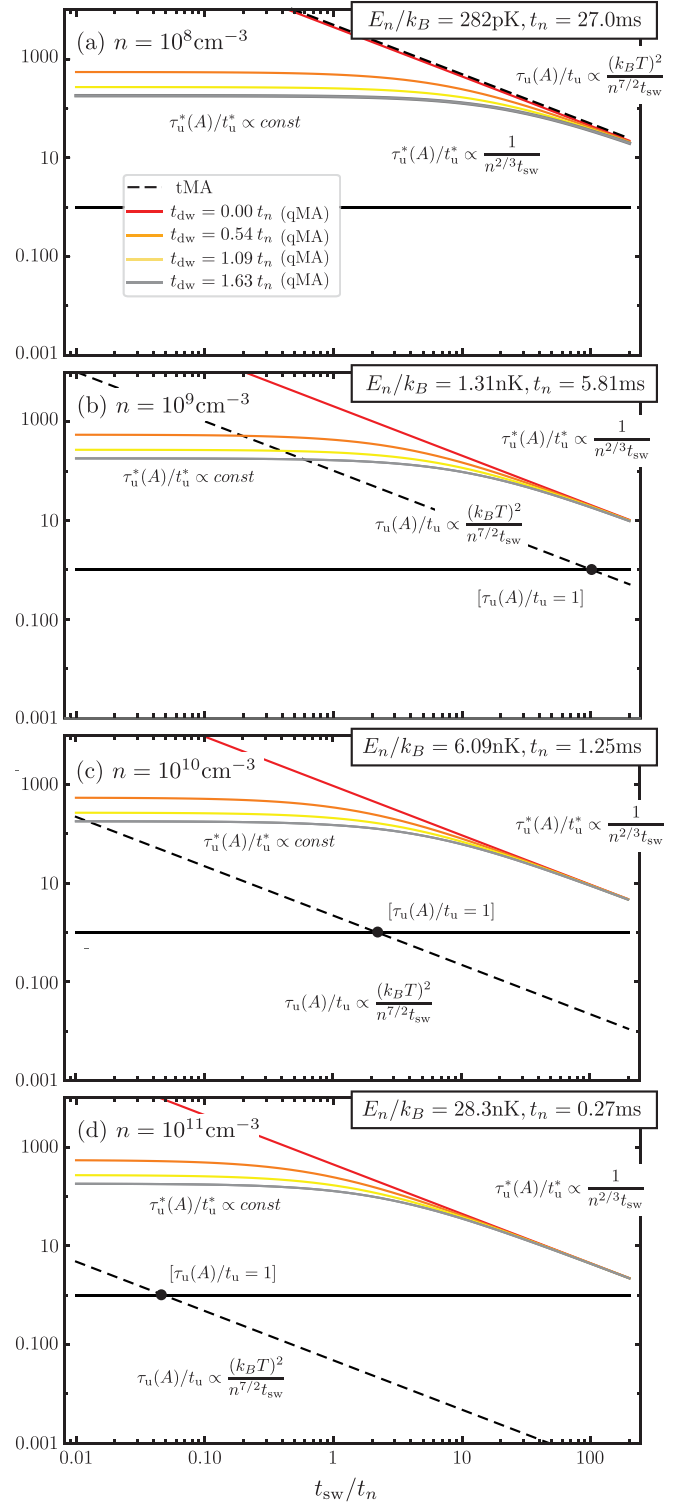$$

FIG. 4. Analysis of the relevant timescales for magneto-association. For TMA, the values for τ_u/t_u calculated from the lifetimes due to RbRbK losses at $T = 100$ pK (black dashed curves) for various densities and a broad range of sweeping times. As n increases, the values of t_{sw} in which $\tau_u/t_u > 1$ becomes quickly more restrictive. For QMA we display the values for τ_u^*/t_u^* (solid curves) for various values of t_{dw}. Regardless of the density, a broad range of t_{sw} satisfies the favorable condition for magneto-association, $\tau_u^*/t_u^* > 1$.

where $\mu_{\mathrm{ad}} = (m_1 + m_2)m_3/(m_1 + m_2 + m_3)$ is the atom-molecule reduced mass. In this case, assuming that the B-field sweep in TMA is performed at constant temperature, the molecular lifetime is simply given by

$$\tau_{\mathrm{u}}(M) = \frac{1}{n\beta_{\mathrm{u}}(T)}$$

$$= \frac{3\pi^{3/2}\mu_{\mathrm{ad}}^{3/2}(k_B T)^{1/2}\hbar^{1/2}}{2\mu^{3/2}(1 - e^{-4\eta})}t_n^{3/2} \propto \frac{(k_B T)^{1/2}}{n}, \quad (18)$$

providing a weaker dependence on temperature and density than those for their atomic counterparts in Eq. (12). From the above equation, the molecular lifetimes due to RbRbK losses at $T = 100$ pK and densities of $10^8/\mathrm{cm}^3$, $10^9/\mathrm{cm}^3$, $10^{10}/\mathrm{cm}^3$, and $10^{11}/\mathrm{cm}^3$ are, respectively, $29t_n$, $14t_n$, $6.3t_n$, and $2.9t_n$, or, equivalently, 0.8 s, 80 ms, 8 ms, and 0.8 ms. These lifetimes should be compared to that of the interaction time [Eq. (7)],

$$\tau_{\mathrm{u}}(M)/t_{\mathrm{u}} \propto \frac{(k_B T)^{1/2}}{n^{4/3}t_{\mathrm{sw}}}. \quad (19)$$

In the case of QMA, assuming that the initial temperature is smaller than E_n, the molecular lifetime is determined by

$$\tau_{\mathrm{u}}^*(M) = \frac{1}{n\beta_{\mathrm{u}}(E_n/k_B)}$$

$$= \frac{3\pi^{3/2}\mu_{\mathrm{ad}}^{3/2}\hbar}{2\mu^{3/2}(1 - e^{-4\eta})}t_n \propto \frac{1}{n^{2/3}}. \quad (20)$$

Here, the lifetimes due to RbRbK losses at $T = 100$ pK is $49t_n$, which for densities of $10^8/\mathrm{cm}^3$, $10^9/\mathrm{cm}^3$, $10^{10}/\mathrm{cm}^3$, and $10^{11}/\mathrm{cm}^3$ becomes 1.3 s, 0.3 s, 62 ms, and 13 ms, respectively. Comparing this lifetime to the interaction time in Eq. (8), we obtain, in the limit of long dwell times, $t_{\mathrm{dw}} \gg t_{\mathrm{u}}$,

$$\tau_{\mathrm{u}}^*(M)/t_{\mathrm{u}}^* \propto \mathrm{const}, \quad (21)$$

while for short dwell times, $t_{\mathrm{dw}} \ll t_{\mathrm{u}}$,

$$\tau_{\mathrm{u}}^*(M)/t_{\mathrm{u}}^* \propto \frac{1}{n^{2/3}t_{\mathrm{sw}}}. \quad (22)$$

The results above lead to conclusions similar to those reached when analyzing the atomic lifetimes. Note that for the particular case of RbK mixtures, the typical molecular lifetimes τ_M^{u} and $\tau_M^{\mathrm{u}*}$ are longer than those for the atomic lifetimes analyzed above.

Overall, the analysis above indicates that the detrimental effects of atomic and molecular losses on magneto-association are, in general, mitigated in the low-density regime, regardless of the magneto-association scheme. The CAL fully takes advantage of this property due to its unique capability to provide ultralow-density samples. The QMA, however, seems to provide a more stable scheme, in particular at higher densities, due to its independence from temperature and the much more favorable ratio between lifetime and interaction times, $\tau_A^{\mathrm{u}*}/t_{\mathrm{u}}^*$. The caveat of using quenches is that the final temperature of the molecular sample will directly depend on the density (via its dependence on E_n), an effect that can, once again, be mitigated at low-densities. Although such prospects are positive with respect to losses in the low-density regime, the question we now focus on is how the actual efficiencies of the two magneto-association schemes compare to each other

in this regime and whether association occurs on timescales shorter than the atomic and molecular losses. We provide such an analysis in the next section.

IV. MOLECULAR ASSOCIATION

In this section we present our numerical simulation for both TMA and QMA near the $^{87}\mathrm{Rb}$-$^{41}\mathrm{K}$ Feshbach resonance at $B_0 = 39.4$ G [42] (Fig. 1). In each case, we select $a_i = -2r_{\mathrm{vdW}}$ ($\approx -144a_0$) and $a_f = 100r_{\mathrm{vdW}}$ ($\approx 7230a_0$), corresponding to $B_i = 63.92$ G and $B_f = 37.89$ G. Therefore, we assume bosonic heteronuclear Feshbach molecules which are substantially larger than previously studied [57,58], which aligns best with CAL's future experiments on microgravity [24]. As a result, most of our studies presented here will be performed for atomic densities in which the average interatomic distances are larger than the molecular size, i.e., $n \leqslant 10^{11}/\mathrm{cm}^3$. We study the molecular fraction in terms of the sweeping time t_{sw}, dwell time t_{dw}, and atomic densities. We note that the qualitative trends in our results do not depend on the particular choices of B_i and B_f, as long as they are chosen to be off resonance, i.e., $1/|k_n a| \gg 1$.

Here, we choose to compute the molecular fraction for four different atomic densities $n = 10^8/\mathrm{cm}^3$, $10^9/\mathrm{cm}^3$, $10^{10}/\mathrm{cm}^3$, and $10^{11}/\mathrm{cm}^3$, thereby covering the density regime available to the CAL environment. Results are displayed in Fig. 5, where dashed lines represent the molecular fractions obtained via TMA, and solid lines show the ones obtained via QMA for different values of t_{dw} [see color-coded legend in Fig. 5(d)]. For each density, we also indicate the corresponding values for E_n and t_n as they characterize the typical energies and timescales of the system at a given density n. These calculations yield a few crucial observations that are valid for all densities considered.

First, as shown in Fig. 5, in the low-density regime QMA produces a higher molecular fraction than TMA within the same value for t_{sw}. This immediately implies the most significant result of this study: within a given t_{sw}, a quench with finite t_{dw} followed by a B-field sweep away from unitarity will, in general, produce a larger molecular fraction than a pure B-field sweep in the same amount of time. Therefore, in order to produce a larger fraction of molecules in the shortest amount of time, QMA is clearly the optimal choice. The faster times for molecular formation within QMA are crucially important since they ensure the mitigation of atomic and molecular losses, in particular for higher densities, as discussed in Sec. III B (see Fig. 4). Figure 5 also indicates that QMA reaches an efficiency of about 80%, reaching this maximum value for smaller values of t_{sw}/t_n as n increases (see points in Fig. 5 marked "max*"). The finite efficiency in QMA is likely to be associated with the nature of the quenched state in Eq. (10), where excited states are more likely to remain in the atomic states than the target molecular state which the B field sweeps away from the interaction region $1/|k_n a| < 1$. A more complete analysis of this topic is beyond the scope of the present study. For TMA, although one would, in theory, expect a nearly 100% efficiency as $t_{\mathrm{sw}} \to \infty$, the results in Fig. 5, along with those for the atomic losses in Fig. 4, clearly show that substantial losses will take place well before this level of efficiency is reached.
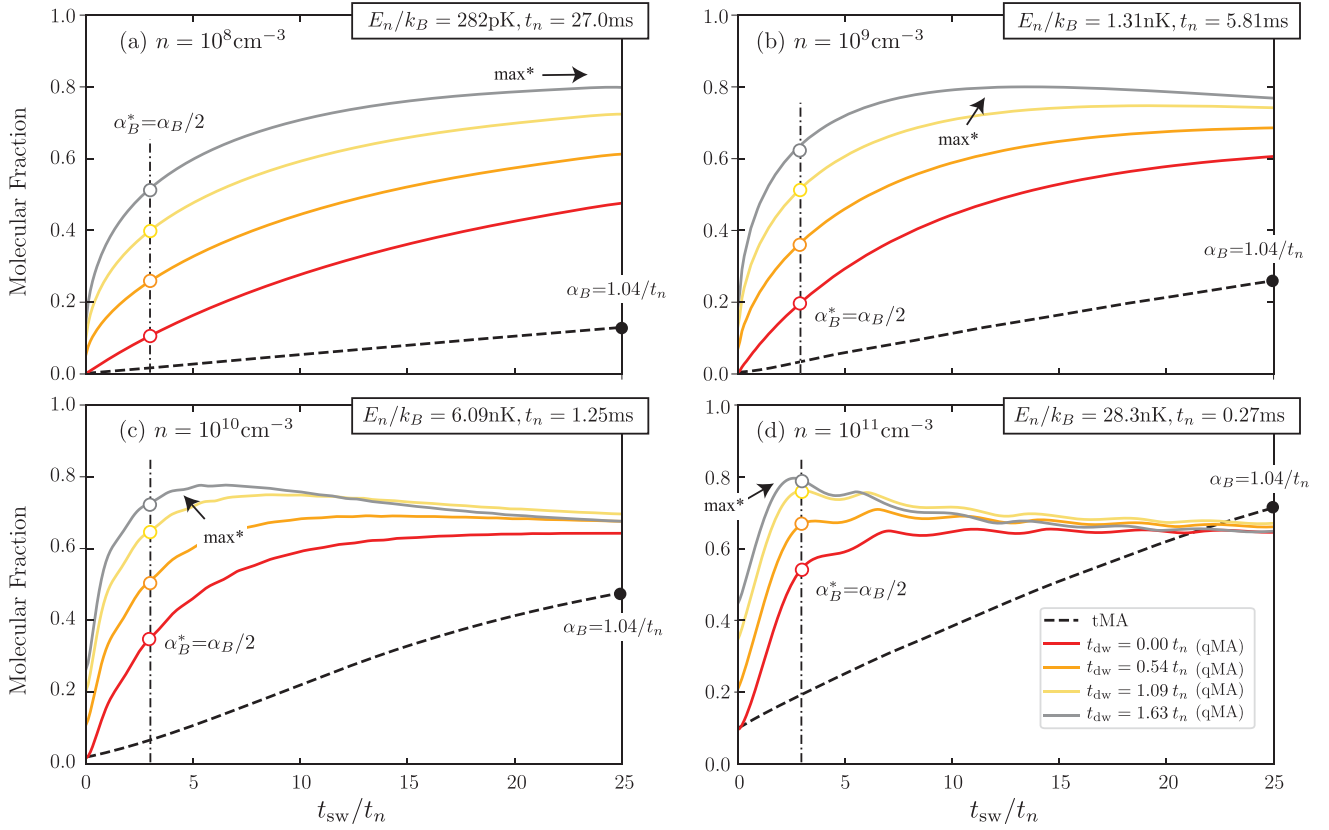
FIG. 5. Fraction of molecules produced as a function of $t_{\rm sw}$ for various densities. The dashed curve represents results for TMA, while solid curves are those for QMA at different dwelling times $t_{\rm dw}$. In all cases the initial and final states are characterized by $a_i = -2r_{\rm vdW}$ and $a_f = 100r_{\rm vdw}$, respectively. Note that at $t_{\rm sw} = 0$, TMA results are identical to those from QMA at $t_{\rm sw} = t_{\rm dw} = 0$. (See the text for more discussions of these results and comparisons). Each panel displays the corresponding values for E_n and t_n.

In order to better understand the physical aspects determining the superiority of QMA over TMA we look at the values of the molecular fraction at $t_{\rm sw} = 0$ in Fig. 5. This value indicates the quality of the overlap between the initial state (prior to the B-field sweeping) and the final molecular state. As shown in Fig. 5, while for TMA and QMA ($t_{\rm dw} = 0$) the molecular fractions are nearly identical, it increases for QMA with $t_{\rm dw}$. This result is consistent with the experimental observations in Ref. [31] and demonstrates that the dwelling time plays an important role in the state preparation by letting correlations evolve in the interaction region $1/|k_n a| < 1$. We note, however, that for $t_{\rm sw} > 0$ the sweeping rates implied in Fig. 5 are, in fact, different. While for the TMA the sweep rate is $\alpha_B = |B_f - B_i|/t_{\rm sw} \approx 26.03$ G/$t_{\rm sw}$, in QMA the rate is $\alpha_B^* = |B_f - B_0|/t_{\rm sw} \approx 1.51$ G/$t_{\rm sw}$. The slower values for α_B^* thus partially explain the higher molecular fraction obtained via QMA for a given value of $t_{\rm sw} > 0$.

In order to make a more direct comparison between the efficiencies of both schemes we should compare, for instance, the molecular fractions obtained for sweeping rates that lead to the same sweeping times within the interaction region, $1/|k_n a| = 1$. Now, considering that for TMA one expends twice the time sweeping in this region than for QMA, we will seek values of $t_{\rm sw}$ in which $\alpha_B^* = \alpha_B/2$. We note, however, that since in TMA and QMA the system experiences interactions differently during the time spent sweeping across $1/|k_n a| < 1$,

our comparison here can provide only a rough analysis. Our comparison is shown in Fig. 5. We indicate the molecular fraction for TMA at $t_{\rm sw} = 25 t_n$ by a solid circle, producing the rate $\alpha_B = 1.04/t_n$. This value should then be compared to those obtained via QMA at $t_{\rm sw} = 2.90 t_n$, as indicated by the open circles in Fig. 5. This analysis again demonstrates that for low densities, as $t_{\rm dw}$ increases, the efficiency of QMA will surpass that of TMA while still providing a much faster scheme to associate atoms into molecules.

In order to illustrate the comparative performance of both association schemes at higher densities and other typical parameters, Fig. 6 shows our simulations for TMA and QMA for an atomic density of $n = 10^{13}$/cm^3. This calculation associates atoms with a Feshbach molecular state with $a = 10r_{\rm vdW}$ and demonstrates again the superiority of QMA in creating molecules at a faster rate. This result indicates that QMA provides a vital tool for molecular creation not only in microgravity but also in typical regimes in ground-based experiments.

V. CONCLUSION

In this paper we have investigated methods to produce molecules via magneto-association near a Feshbach resonance, focusing on the low-density regime relevant to the microgravity environment of CAL. Based on the trends
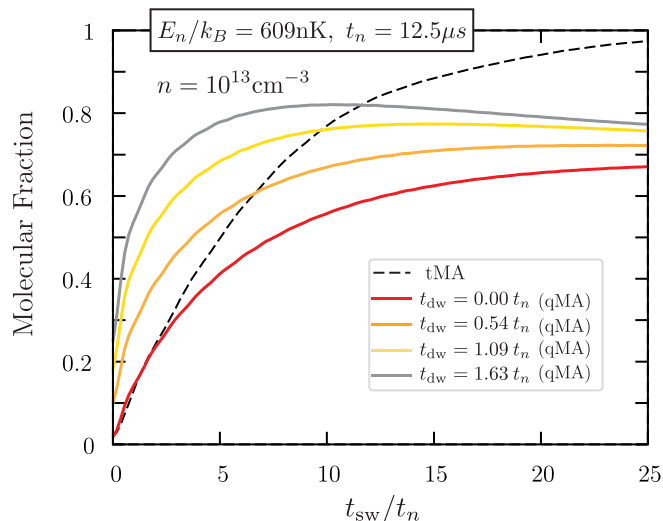
FIG. 6. Fraction of molecules produced as a function of t_{sw} for $n = 10^{13}/\text{cm}^3$. The dashed curve represents results for TMA, while solid curves are those for QMA at different dwelling times t_{dw}. In all cases the initial and final states are characterized by $a_i = -2r_{vdW}$ and $a_f = 10r_{vdW}$, respectively.

discovered in our computations, we conclude that a QMA can generally be made superior to TMA. Within QMA, we found that the dwelling time in the interaction region, $1/|k_n a| < 1$,

allows for correlations to develop, thus providing a much more efficient scheme for association of atoms in molecules. Our results show that QMA allows for a much higher association efficiency ($\sim 80\%$) within considerably faster timescales than TMA. The higher association rates in QMA allows for further mitigation of atomic and molecular losses, regardless of the density regime.

In further studies of molecular production, several more complicated aspects of the system could be investigated. For instance, one could introduce dynamically the various loss processes dependent on scattering length and attempt to optimize molecular production constrained by the loss timescales in a more rigorous way than presented here. Also, while the analysis in this study considered purely two-body interactions, one could extend the analysis by incorporating three-body effects, which would then have to consider both Rb-Rb-K and Rb-K-K interactions, as well as the formation of triatomic Efimov states existing in the system [39].

ACKNOWLEDGMENTS

[1] K.-A. B. Soderberg, N. Gemelke, and C. Chin, Ultracold molecules: Vehicles to scalable quantum information processing, New J. Phys. **11**, 055022 (2009).

[2] L. D. Carr, D. DeMille, R. V. Krems, and J. Ye, Cold and ultracold molecules: Science, technology and applications, New J. Phys. **11**, 055049 (2009).

[3] J. W. Park, Z. Z. Yan, H. Loh, S. A. Will, and M. W. Zwierlein, Second-scale nuclear spin coherence time of ultracold ^{23}Na^{40}K molecules, Science **357**, 372 (2017).

[4] K.-K. Ni, T. Rosenband, and D. D. Grimes, Dipolar exchange quantum logic gate with polar molecules, Chem. Sci. **9**, 6830 (2018).

[5] L. Anderegg, L. W. Cheuk, Y. Bao, S. Burchesky, W. Ketterle, K.-K. Ni, and J. M. Doyle, An optical tweezer array of ultracold molecules, Science **365**, 1156 (2019).

[6] R. V. Krems, Cold controlled chemistry, Phys. Chem. Chem. Phys. **10**, 4079 (2008).

[7] G. Quéméner and P. S. Julienne, Ultracold molecules under control! Chem. Rev. **112**, 4949 (2012).

[8] M.-G. Hu, Y. Liu, D. D. Grimes, Y.-W. Lin, A. H. Gheorghe, R. Vexiau, N. Bouloufa-Maafa, O. Dulieu, T. Rosenband, and K.-K. Ni, Direct observation of bimolecular reactions of ultracold KrB molecules, Science **366**, 1111 (2019).

[9] G. Valtolina, K. Matsuda, W. G. Tobias, J.-R. Li, L. De Marco, and J. Ye, Dipolar evaporation of reactive molecules to below the Fermi temperature, Nature (London) **588**, 239 (2020).

[10] K.-K. Ni, S. Ospelkaus, M. H. G. de Miranda, A. Pe'er, B. Neyenhuis, J. J. Zirbel, S. Kotochigova, P. S. Julienne, D. S. Jin,

and J. Ye, A high phase-space-density gas of polar molecules, Science **322**, 231 (2008).

[11] J. G. Danzl, M. J. Mark, E. Haller, M. Gustavsson, R. Hart, J. Aldegunde, J. M. Hutson, and H.-C. Nägerl, An ultracold high-density sample of rovibronic ground-state molecules in an optical lattice, Nat. Phys. **6**, 265 (2010).

[12] S. Ospelkaus, K.-K. Ni, D. Wang, M. H. G. de Miranda, B. Neyenhuis, G. Quéméner, P. S. Julienne, J. L. Bohn, D. S. Jin, and J. Ye, Quantum-state controlled chemical reactions of ultracold potassium-rubidium molecules, Science **327**, 853 (2010).

[13] K. K. Ni, S. Ospelkaus, D. Wang, G. Quéméner, B. Neyenhuis, M. H. G. de Miranda, J. L. Bohn, J. Ye, and D. S. Jin, Dipolar collisions of polar molecules in the quantum regime, Nature (London) **464**, 1324 (2010).

[14] Y. Wang, J. P. D'Incao, and C. H. Greene, Efimov Effect for Three Interacting Bosonic Dipoles, Phys. Rev. Lett. **106**, 233201 (2011).

[15] Y. Wang, J. P. D'Incao, and C. H. Greene, Universal Three-Body Physics for Fermionic Dipoles, Phys. Rev. Lett. **107**, 233201 (2011).

[16] C. Chin and V. V. Flambaum, Enhanced Sensitivity to Fundamental Constants in Ultracold Atomic and Molecular Systems near Feshbach Resonances, Phys. Rev. Lett. **96**, 230801 (2006).

[17] C. Chin, V. V. Flambaum, and M. G. Kozlov, Ultracold molecules: New probes on the variation of fundamental constants, New J. Phys. **11**, 055048 (2009).

[18] A. Borschevsky, K. Beloy, V. V. Flambaum, and P. Schwerdtfeger, Sensitivity of ultracold-atom scattering experiments to variation of the fine-structure constant, Phys. Rev. A **83**, 052706 (2011).

[19] T. Köhler, K. Góral, and P. S. Julienne, Production of cold molecules via magnetically tunable feshbach resonances, Rev. Mod. Phys. **78**, 1311 (2006).

[20] T. M. Hanna, T. Köhler, and K. Burnett, Association of molecules using a resonantly modulated magnetic field, Phys. Rev. A **75**, 013606 (2007).

[21] T. V. Tscherbul, T. Calarco, I. Lesanovsky, R. V. Krems, A. Dalgarno, and J. Schmiedmayer, rf-field-induced Feshbach resonances, Phys. Rev. A **81**, 050701(R) (2010).

[22] D. J. Owens, T. Xie, and J. M. Hutson, Creating Feshbach resonances for ultracold molecule formation with radio-frequency fields, Phys. Rev. A **94**, 023619 (2016).

[23] Y. Ding, J. P. D'Incao, and C. H. Greene, Effective control of cold collisions with radio-frequency fields, Phys. Rev. A **95**, 022709 (2017).

[24] J. P. D'Incao, M. Krutzik, E. Elliott, and J. R. Williams, Enhanced association and dissociation of heteronuclear Feshbach molecules in a microgravity environment, Phys. Rev. A **95**, 012701 (2017).

[25] P. Giannakeas, L. Khaykovich, J.-M. Rost, and C. H. Greene, Nonadiabatic Molecular Association in Thermal Gases Driven by Radio-Frequency Pulses, Phys. Rev. Lett. **123**, 043204 (2019).

[26] J. Cubizolles, T. Bourdel, S. J. J. M. F. Kokkelmans, G. V. Shlyapnikov, and C. Salomon, Production of Long-Lived Ultracold Li_2 Molecules from a Fermi Gas, Phys. Rev. Lett. **91**, 240401 (2003).

[27] J. Herbig, T. Kraemer, M. Mark, T. Weber, C. Chin, H.-C. Nägerl, and R. Grimm, Preparation of a pure molecular quantum gas, Science **301**, 1510 (2003).

[28] C. A. Regal, C. Ticknor, J. L. Bohn, and D. S. Jin, Creation of ultracold molecules from a Fermi gas of atoms, Nature (London) **424**, 47 (2003).

[29] K. E. Strecker, G. B. Partridge, and R. G. Hulet, Conversion of an Atomic Fermi Gas to a Long-Lived Molecular Bose Gas, Phys. Rev. Lett. **91**, 080406 (2003).

[30] S. Dürr, T. Volz, A. Marte, and G. Rempe, Observation of Molecules Produced from a Bose-Einstein Condensate, Phys. Rev. Lett. **92**, 020406 (2004).

[31] M. Mark, T. Kraemer, J. Herbig, C. Chin, H.-C. Nägerl, and R. Grimm, Efficient creation of molecules from a cesium Bose-Einstein condensate, Europhys. Lett. **69**, 706 (2005).

[32] C. Chin, R. Grimm, P. Julienne, and E. Tiesinga, Feshbach resonances in ultracold gases, Rev. Mod. Phys. **82**, 1225 (2010).

[33] K. Bergmann, N. V. Vitanov, and B. W. Shore, Perspective: Stimulated Raman adiabatic passage: The status after 25 years, J. Chem. Phys. **142**, 170901 (2015).

[34] E. R. Elliott, M. C. Krutzik, J. R. Williams, R. J. Thompson, and D. C. Aveline, NASA's Cold Atom Lab (CAL): System development and ground test status, npj Microgravity **4**, 16 (2018).

[35] D. C. Aveline, J. R. Williams, E. R. Elliott, C. Dutenhoffer, J. R. Kellogg, J. M. Kohel, N. E. Lay, K. Oudrhiri, R. F. Shotwell, N. Yu, and R. J. Thompson, Observation of Bose–Einstein condensates in an earth-orbiting research lab, Nature (London) **582**, 193 (2020).

[36] J. Williams, S. W. Chiow, N. Yu, and H. Müller, Quantum test of the equivalence principle and space-time aboard the international space station, New J. Phys. **18**, 025018 (2016).

[37] P. Asenbaum, C. Overstreet, M. Kim, J. Curti, and M. A. Kasevich, Atom-Interferometric Test of the Equivalence Principle at the 10^{-12} level, Phys. Rev. Lett. **125**, 191101 (2020).

[38] M. S. Safronova, D. Budker, D. DeMille, D. F. J. Kimball, A. Derevianko, and C. W. Clark, Search for new physics with atoms and molecules, Rev. Mod. Phys. **90**, 025008 (2018).

[39] C. E. Klauss, X. Xie, C. Lopez-Abadia, J. P. D'Incao, Z. Hadzibabic, D. S. Jin, and E. A. Cornell, Observation of Efimov Molecules Created from a Resonantly Interacting Bose Gas, Phys. Rev. Lett. **119**, 143401 (2017).

[40] J. P. D'Incao, J. Wang, and V. E. Colussi, Efimov Physics in Quenched Unitary Bose Gases, Phys. Rev. Lett. **121**, 023401 (2018).

[41] A. Derevianko, J. F. Babb, and A. Dalgarno, High-precision calculations of van der Waals coefficients for heteronuclear alkali-metal dimers, Phys. Rev. A **63**, 052704 (2001).

[42] A. Simoni, M. Zaccanti, C. D'Errico, M. Fattori, G. Roati, M. Inguscio, and G. Modugno, Near-threshold model for ultracold KRb dimers from interisotope Feshbach spectroscopy, Phys. Rev. A **77**, 052705 (2008).

[43] B. Borca, D. Blume, and C. H. Greene, A two-atom picture of coherent atom–molecule quantum beats, New J. Phys. **5**, 111 (2003).

[44] K. Góral, T. Köhler, S. A. Gardiner, E. Tiesinga, and P. S. Julienne, Adiabatic association of ultracold molecules via magnetic-field tunable interactions, J. Phys. B **37**, 3457 (2004).

[45] J. von Stecher and C. H. Greene, Spectrum and Dynamics of the BCS-BEC Crossover from a Few-Body Perspective, Phys. Rev. Lett. **99**, 090402 (2007).

[46] A. G. Sykes, J. P. Corson, J. P. D'Incao, A. P. Koller, C. H. Greene, A. M. Rey, K. R. A. Hazzard, and J. L. Bohn, Quenching to unitarity: Quantum dynamics in a three-dimensional Bose gas, Phys. Rev. A **89**, 021601(R) (2014).

[47] J. P. Corson and J. L. Bohn, Bound-state signatures in quenched Bose-Einstein condensates, Phys. Rev. A **91**, 013616 (2015).

[48] V. E. Colussi, J. P. Corson, and J. P. D'Incao, Dynamics of Three-Body Correlations in Quenched Unitary Bose Gases, Phys. Rev. Lett. **120**, 100401 (2018).

[49] E. Hodby, S. T. Thompson, C. A. Regal, M. Greiner, A. C. Wilson, D. S. Jin, E. A. Cornell, and C. E. Wieman, Production Efficiency of Ultracold Feshbach Molecules in Bosonic and Fermionic Systems, Phys. Rev. Lett. **94**, 120402 (2005).

[50] S. T. Thompson, E. Hodby, and C. E. Wieman, Ultracold Molecule Production Via a Resonant Oscillating Magnetic Field, Phys. Rev. Lett. **95**, 190404 (2005).

[51] S. B. Papp and C. E. Wieman, Observation of Heteronuclear Feshbach Molecules from a ^{85}Rb–^{87}Rb Gas, Phys. Rev. Lett. **97**, 180404 (2006).

[52] C. W. Clark, The calculation of non-adiabatic transition probabilities, Phys. Lett. A **70**, 295 (1979).

[53] J. E. Bækhøj, O. I. Tolstikhin, and L. B. Madsen, "Slow" time discretization: A versatile time propagator for the time-dependent Schrödinger equation, J. Phys. B **47**, 075007 (2014).

[54] J. P. D'Incao, Few-body physics in resonantly interacting ultracold quantum gases, J. Phys. B **51**, 043001 (2018).

[55] G. Barontini, C. Weber, F. Rabatti, J. Catani, G. Thalhammer, M. Inguscio, and F. Minardi, Observation of Heteronuclear Atomic Efimov Resonances, Phys. Rev. Lett. **103**, 043201 (2009).

[56] P. Makotyn, C. E. Klauss, D. L. Goldberger, E. A. Cornell, and D. S. Jin, Universal dynamics of a degenerate unitary Bose gas, Nat. Phys. **10**, 116 (2014).

[57] C. Klempt, T. Henninger, O. Topic, M. Scherer, L. Kattner, E. Tiemann, W. Ertmer, and J. J. Arlt, Radio-frequency association of heteronuclear Feshbach molecules, Phys. Rev. A **78**, 061602(R) (2008).

[58] C. Weber, G. Barontini, J. Catani, G. Thalhammer, M. Inguscio, and F. Minardi, Association of ultracold double-species bosonic molecules, Phys. Rev. A **78**, 061601(R) (2008).